actuators

MDPI

Article

Self-Sensing Approach for Semi-Active Control of Variable Damping Electromagnetic Suspension System

Chao Fu [1], Pengfei Liu [1,*], Jianqiang Yu [2,*], An Qin [3] and Donghong Ning [1]

[1] College of Engineering, Ocean University of China, Qingdao 266100, China; fuchao@stu.ouc.edu.cn (C.F.); ningdonghong@ouc.edu.cn (D.N.)
[2] China Nanhu Academy of Electronics and Information Technology, Jiaxing 314001, China
[3] College of Mechanical and Vehicle Engineering, Hunan University, Changsha 410082, China; anqin@hnu.edu.cn
* Correspondence: liupengfei@ouc.edu.cn (P.L.); yjq2012@alu.cqu.edu.cn (J.Y.)

Abstract: This paper combines the Kalman filter observer with self-sensing technology and integrates it into the electromagnetic damper (EMD), estimating the displacement and velocity of the EMD based on the three-phase voltage generated by the permanent magnet synchronous motor (PMSM). The self-sensing performance of the EMD is verified through theoretical analysis and experimental results. A vehicle suspension vibration control system composed of one-quarter vehicle electromagnetic suspension (EMS), a acceleration damping driven control (ADDC) algorithm, and a vibration excitation platform is established to test the vibration control performance of the self-sensing EMS. The experimental results show that under random road excitation, compared to passive suspension, the self-sensing-based ADDC reduced the vehicle vertical acceleration of the vehicle suspension, with a 28.92% decrease in the root mean square (RMS) value of the vehicle vertical acceleration. This verifies the effectiveness of the self-sensing capability of the EMS system. Incorporating self-sensing technology into the EMS system improves the vibration reduction performance of the suspension.

Keywords: semi-active control; self-sensing; variable damping; electromagnetic suspension

check for updates

Citation: Fu, C.; Liu, P.; Yu, J.; Qin, A.; Ning, D. Self-Sensing Approach for Semi-Active Control of Variable Damping Electromagnetic Suspension System. *Actuators* **2024**, *13*, 480. https://doi.org/10.3390/act13120480

Academic Editors: Seongjin Yim and Kanghyun Nam

Received: 7 October 2024
Revised: 16 November 2024
Accepted: 26 November 2024
Published: 27 November 2024

Copyright: © 2024 by the authors. Licensee MDPI, Basel, Switzerland. This article is an open access article distributed under the terms and conditions of the Creative Commons Attribution (CC BY) license (https://creativecommons.org/licenses/by/4.0/).

1. Introduction

Semi-active suspensions combine the advantages of both passive and active suspensions, offering suspension performance similar to active systems while maintaining low cost and energy consumption. Therefore, semi-active suspension technology provides an alternative research direction for improving ride comfort. Currently, actuators made of magnetorheological materials are applied in vehicle suspension systems for vibration reduction [1,2]. Though the traditional semi-active vehicle suspension consumes less power than the active one, it still needs energy input. An electromagnetic damper (EMD) can harvest the energy from road vibration instead of consuming it [3]. Therefore, to achieve real-time control of the mechanical characteristics of the semi-active suspension, this paper adopts an electromagnetic damper (EMD) composed of a ball screw and a permanent magnet synchronous motor (PMSM) to form an electromagnetic suspension (EMS) system. By controlling the load components in the circuit, the EMS exhibits mechanically controllable damping characteristics.

In traditional suspension control methods, suspension displacement and velocity are considered known parameters, often relying on displacement sensors to obtain suspension displacement and velocity information [4], such as linear displacement sensors [5,6]. However, these sensors are expensive and require a large amount of installation space, making the installation process quite inconvenient [7], which increases system cost and complexity. To address these issues, some experts and researchers use state estimation methods [8]. Ren et al. [9] developed a suspension state observer based on unscented Kalman filtering, which improved the robustness of the control strategy and adapted to

different types of road disturbances. Pan et al. [10] proposed a nonlinear tracking control strategy with an Extended State Observer (ESO) for vehicle active suspension to improve ride comfort. Wang et al. [11] introduced an LPV Kalman filter to estimate state variables in semi-active air suspension systems that are difficult or impossible to measure physically. Zhang et al. [12] designed a Luenberger state observer to provide unmeasurable state parameters for the air suspension controller. Xia et al. [13] proposed a hybrid controller to estimate seat suspension friction using accelerations, relative displacements, and circuit currents that can be measured in practice, and compensated for frictional effects in an H∞ controller. Although these methods have demonstrated their effectiveness, they still rely on sensor inputs, making them susceptible to fluctuations and noise, which affects suspension performance.

Self-sensing technology offers a new solution to these problems [14,15]. Verma et al. [16] present a self-sensing electromagnetic actuator for the vibration control of flexible structures. The back electromotive force generated in the coil is measured to evaluate the velocity and displacement of the structure. Yao et al. [17] present a virtual phase torque diagram method based on a self-sensing motor drive system to address the issue in electromechanical system diagnostics where traditional vibration analysis methods are affected by the positioning of additional sensors. Hu et al. [18] present a novel magnetorheological damper based on integrated linear variable differential sensor technology with self-sensing ability. Deng et al. [19] present a magnetorheological automobile damper with a self-sensing function. The self-sensing performance of the magnetorheological automobile damper is verified from the theoretical analysis and experimental results, and the vibration control performance of the self-sensing magnetorheological automobile damper is tested. By applying self-sensing technology, dampers can independently collect data on suspension displacement and velocity, which will greatly reduce system costs, save suspension space, and reduce the need for sensors in the suspension system, thereby improving the stability and controllability of the suspension system. Currently, there are certain fluctuation errors in self-sensing technology. Considering the characteristics of EMS, integrating state estimation with self-sensing technology would have greater practical application value.

This paper applies self-sensing technology to electromagnetic suspension, estimating suspension displacement and suspension velocity without the need for external sensor signal input, and provides the data to the controller to achieve semi-active control of the suspension. The main contributions of this paper are listed as follows.

- Based on the characteristics of electromagnetic suspension, the Kalman filter observer is combined with self-sensing technology to estimate suspension displacement and velocity, and its accuracy is verified through experiments.
- The self-sensing EMD is tested on a one-quarter vehicle testing platform to verify the vibration-damping performance of the self-sensing semi-active EMS.

The subsequent sections of this paper are structured as follows. Section 2 presents the variable damping electromagnetic suspension system. Section 3 presents the principles of self-sensing and provides experimental verification. The controller design is shown in Section 4. The experimental evaluations are presented in Section 5. Finally, Section 6 presents the conclusions of this research.

2. Variable Damping Electromagnetic Suspension System

2.1. Overview of EMS System

As shown in Figure 1, the EMS system connects the EMD to the vehicle body and the unsprung mass through the top and bottom mounting rings, respectively. When the vehicle travels on uneven road surfaces, road excitations are transmitted from the wheel to the vehicle suspension, resulting in linear reciprocating motion between the vehicle body and the unsprung mass. The EMD converts this linear motion into the rotational motion of the motor through a ball screw mechanism. According to Faraday's law of electromagnetic induction, motor rotation generates electromotive force (EMF), which can produce electrical circuit currents. By incorporating a variable resistance module into the external circuit

of the motor and using a controller to send signals to change the resistance value of the variable resistance module, the EMD can achieve variable damping characteristics, forming a variable damping electromagnetic suspension (VD-EMS) system. This study's variable damping function is based on the controllable damping characteristics of the Panasonic 400W PMSM(MSMF042L1U2M). An electromagnetic damper circuit with variable damping is established using the PMSM. The three-phase voltage, internal resistance, and inductance of the three-phase PMSM can be equivalent to a unidirectional DC circuit through a three-phase rectifier, as shown in Figure 2. By connecting the variable resistance module in series with the DC circuit and adjusting the resistance value, the current in the circuit can be altered, thereby changing the damping characteristics of the EMD.

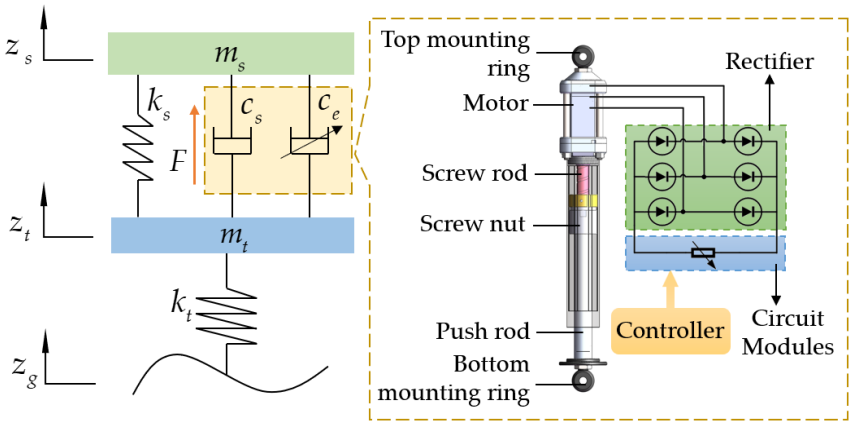

Figure 1. EMD suspension system structure.

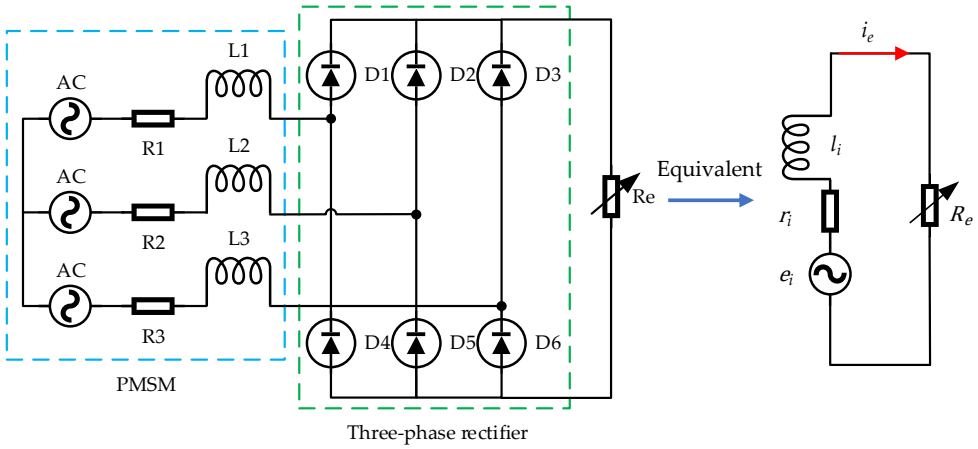

Figure 2. Equivalent principle of the PMSM circuit.

2.2. Principle of EMD Variable Damping

According to the previous text, the circuit is simplified into a DC circuit with a voltage e_i, resistance r_i, and inductance l_i, as shown in Figure 2.

In the closed circuit of Figure 2, the relative motion between the stator and rotor of the PMSM generates an EMF:

$$e_i = k_e \omega_m \tag{1}$$

where k_e is the motor voltage constant and ω_m is the angular velocity of the motor rotor.

According to Ohm's law for the closed circuit, the circuit's current i_e is given by the following equation:

$$i_e = \frac{e_i}{r_i + R_e} \tag{2}$$

where r_i is the internal resistance of the motor and R_e is the resistance value of the variable resistance module.

In the PMSM, this current generates an electromagnetic torque T_e:

$$T_e = k_i i_e \tag{3}$$

where k_i is the torque constant, approximately equal to k_e.

Thus, the electromagnetic force F_e generated by the EMD can be obtained by the following equation:

$$F_e = r_g^2 k_i^2 \frac{v_m}{r_i + R_e} \tag{4}$$

where r_g is the transmission ratio from vertical to rotational motion of the ball screw, related to the lead l of the screw, where $r_g = 2\pi/l$, v_m is the relative velocity of the EMD and $v_m = \omega_m / r_g$.

Therefore, the variable damping c_e of the EMD system can be obtained by the following equation:

$$c_e = \frac{r_g^2 k_i^2}{r_i + R_e} \tag{5}$$

According to Equation (5), variable damping can be achieved by adjusting the resistance in the circuit.

2.3. Characteristic Experiment of EMD

The designed EMD is installed on a suspension test platform for characteristic testing, as shown in Figure 3. In the test experiment, a sinusoidal excitation is applied, $x = 0.02\,sin(3\,\pi t)$. The characteristic test aims to verify the effectiveness of controlling the EMD damping by changing the external circuit resistance. Resistors of 2 Ω, 3 Ω, 8 Ω, and 15 Ω are connected to the circuit. Figure 4a shows the force–displacement characteristic curves (indicator characteristic curve) of the EMD at different resistances. As the connected resistance increases, the area enclosed by the characteristic curve decreases. The area of the characteristic curve represents the change in the damping coefficient because it reflects the variation in the energy output of the EMD. For the same motion velocity, if the energy output changes over the same period, the damping coefficient of the EMD changes accordingly. Figure 4b shows the force–velocity characteristic curves of the EMD under different resistances, where the slope of the curves represents the damping coefficient of the EMD. As the connected resistance gradually increases, the slope decreases, indicating a reduction in the damping coefficient. Figure 5 illustrates the changes in the voltage across the load and the current in the external circuit as the load resistance varies. As the load resistance increases, the voltage gradually rises, while the current gradually decreases.

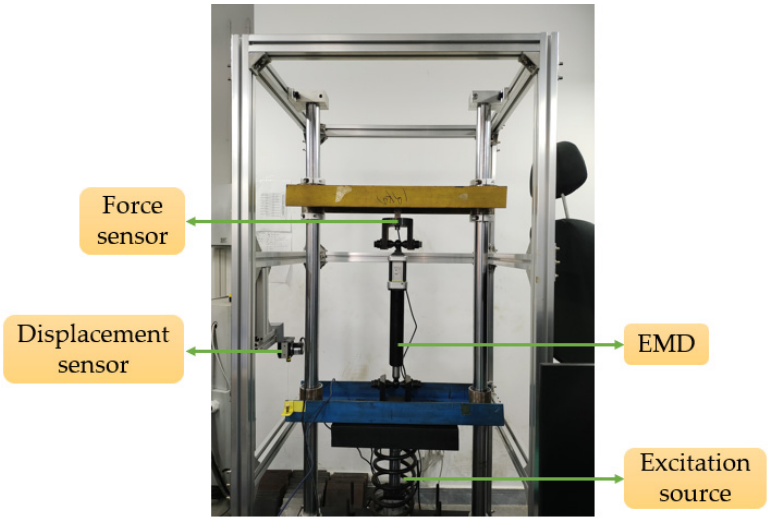

Figure 3. Characteristic testing of EMD.

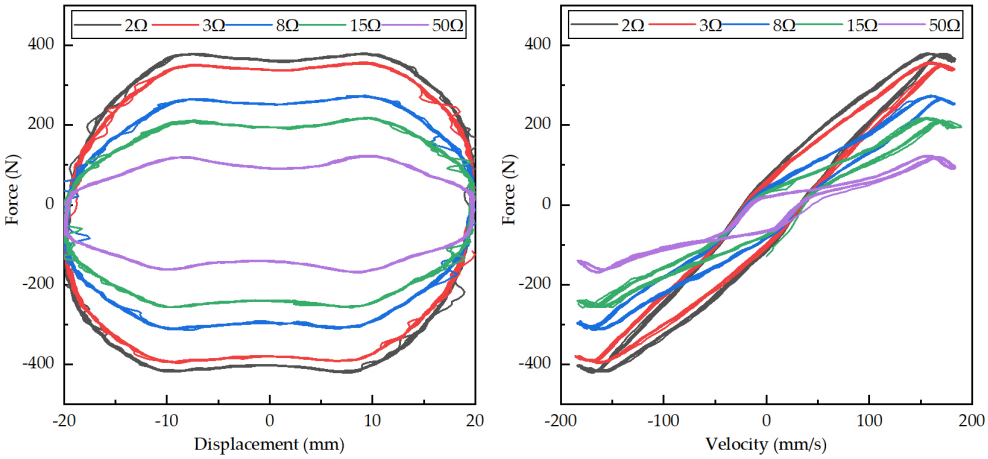

Figure 4. Characteristic curves of EMD: (**a**) force-displacement characteristic curves; (**b**) force-velocity characteristic curves.

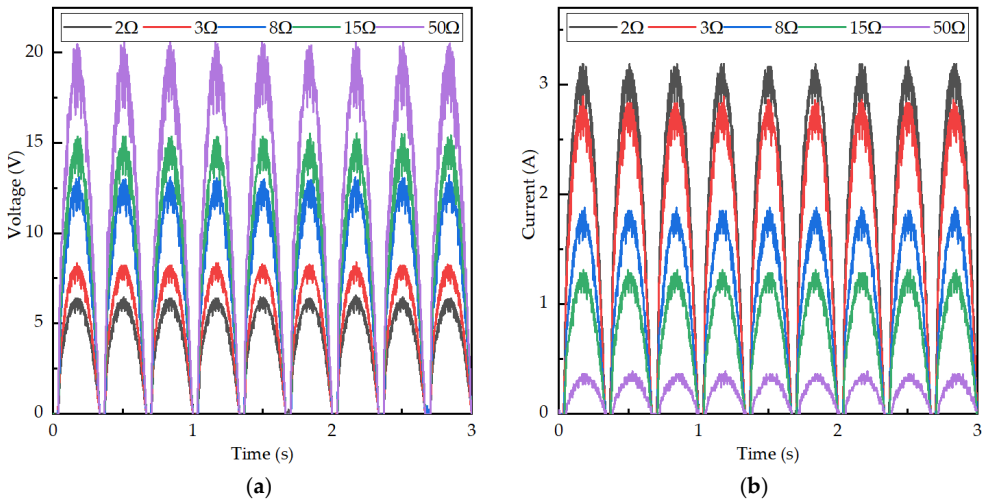

Figure 5. (**a**) Voltage variation curves; (**b**) current variation curves.

The above experimental results demonstrate that by changing the resistance of the external circuit, variable damping can be achieved. The damping adjustment is achieved by controlling the current in the coil through changes in the load.

3. Self-Sensing of VD-EMS System

3.1. Analysis of the Principle of Self-Sensing

The suspension self-sensing means that the relative displacement and relative velocity of the suspension can be estimated by the three-phase induced voltage of the PMSM without the help of external sensors. Based on the working principle, the encoder generates A/B phase pulses during operation. There is a phase difference between the A/B phase pulses, as shown in Figure 6. Assuming that when phase A leads phase B, the motor rotates forward, as shown in Figure 6a, then when phase B leads phase A, the motor reverses, as shown in Figure 6b.

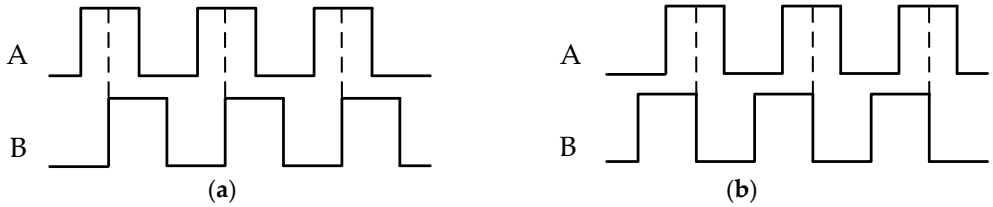

Figure 6. A/B phase pulse: (**a**) phase A leads phase B; (**b**) phase B leads phase A.

In the EMD, a PMSM is used as a generator, converting the up-and-down vibration of the suspension into the rotation of the motor rotor. This rotation cuts through magnetic flux lines, generating an EMF. Analogous to the working principle of an encoder, converting the voltage of the PMSM into pulse form allows estimation of the motor's rotational direction, thereby obtaining the suspension's movement direction, which in turn enables estimation of suspension displacement and velocity. The self-sensing working principle is illustrated in Figure 7.

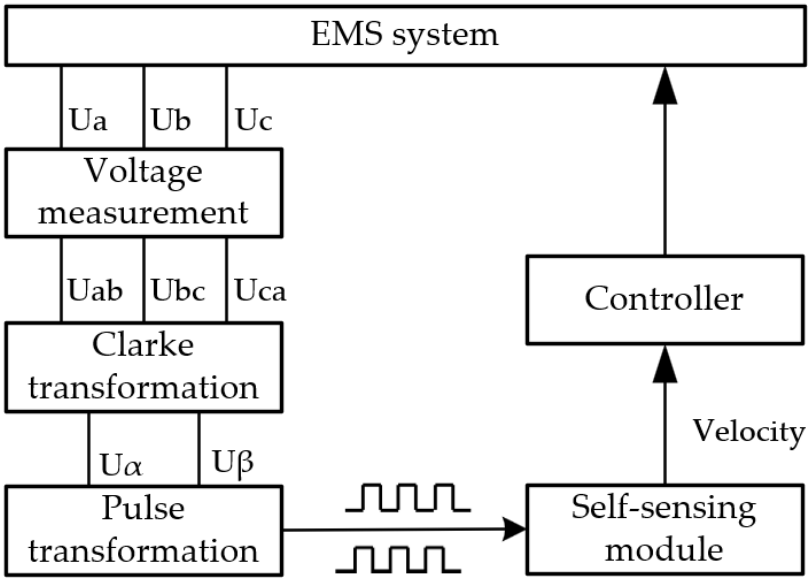

Figure 7. Self-sensing working principle.

The PMSM is connected in a star configuration, which can be simplified as three internal voltage sources, three internal resistors, and three inductors. When the motor rotates, it generates three-phase approximately sinusoidal voltages [20]. Due to the complexity of handling three-phase sinusoidal voltages, it is necessary to equivalently transform it into a stationary α-β coordinate system using the amplitude-invariant Clarke transformation, which can be expressed as [21]

$$\begin{bmatrix} U_\alpha \\ U_\beta \end{bmatrix} = \begin{bmatrix} \frac{2}{3} & -\frac{1}{3} & -\frac{1}{3} \\ 0 & \frac{\sqrt{3}}{3} & \frac{\sqrt{3}}{3} \end{bmatrix} \begin{bmatrix} U_{ab} \\ U_{bc} \\ U_{ca} \end{bmatrix} \tag{6}$$

In this expression, U_α and U_β represent the voltages in the α-β coordinate system respectively. The voltages in the α–β coordinate system can be represented in the form of pulses. Through the above transformation, the three-phase voltage signals generated by the servo motor can be converted into two-phase pulse signals, as shown in Figure 8. By applying the two-phase pulse signal, the relative displacement and relative velocity of the suspension can be estimated.

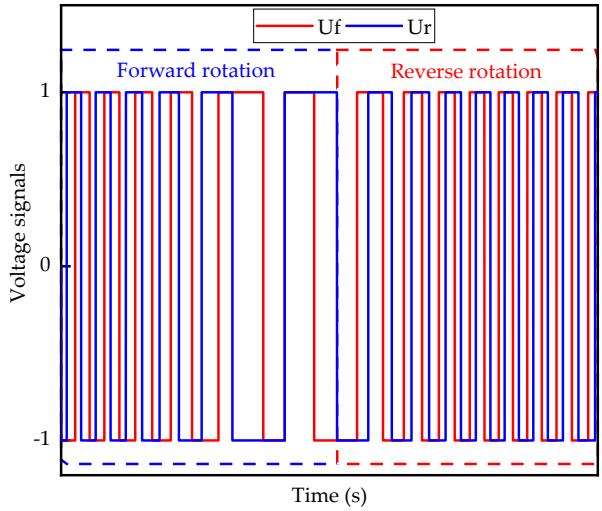

Figure 8. Voltage pulse signal of the stationary coordinate system.

3.2. Suspension Displacement and Velocity Estimation

According to Figure 8, the number of rising and falling edge pulses generated for each rotation of the motor can be calculated using the following equation:

$$n_p = 4p \tag{7}$$

where n_p represents the number of rising and falling edges within a rotation period, and p is the number of pole pairs of the motor; the motor pole pair number selected in this paper is 5.

When the motor is rotating forward, U_f leads U_r; while it is in reverse rotation, it is the opposite, as shown in Figure 8. By counting both forward and reverse pulses, the relationship between the motor angle and the pulse count is obtained as follows:

$$\theta_m = \frac{2\pi}{n_p} n_s \tag{8}$$

where n_s is the sum of the number of forward and reverse voltage pulses.

In EMD, the ball screw can convert the motor's rotational angle into suspension displacement. Therefore, by estimating the motor's rotational angle, the suspension displacement can be determined as follows:

$$d_s = \theta_m \left(\frac{l}{2\pi} \right) \tag{9}$$

Therefore, the speed of the permanent magnet synchronous motor can be obtained by the following equation:

$$\omega = \frac{2\pi}{p\Delta t} \tag{10}$$

where Δt is the time difference between two consecutive pulses.

Similarly, by estimating the motor's angular velocity, the relative velocity of the suspension can be determined as follows:

$$v_m = \omega_m \left(\frac{l}{2\pi} \right) \tag{11}$$

To evaluate the estimation performance of the self-sensing algorithm, as shown in Figure 3, the designed EMD is installed on a suspension vehicle test platform for experimental validation. The accuracy of displacement and velocity estimations is verified under

sinusoidal road surface excitation. In the experiments, a sinusoidal excitation is applied: $x = 0.015\,sin(2\,\pi t)$. To obtain the three-phase voltage, a voltage measurement module is used to collect the three-phase voltage of the PMSM before rectification. Due to significant noise interference in the collected voltage signal, which affects subsequent voltage variations, a Butterworth low-pass filter is applied before signal acquisition. Figure 9 shows a comparison of the actual and estimated values of the suspension's relative displacement and relative velocity under sinusoidal road excitation.

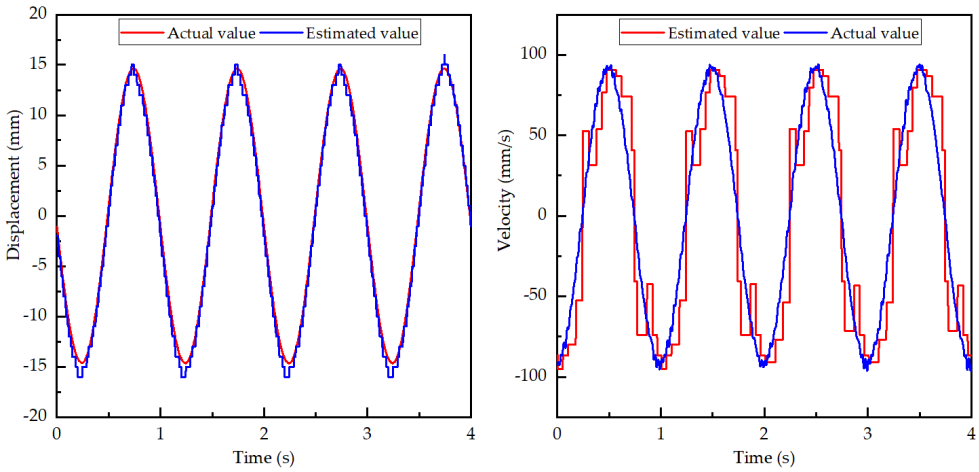

Figure 9. Comparison between estimated value and actual value under sine excitation: (**a**) displacement; (**b**) velocity.

The Root Mean Square Error (RMSE) is a commonly used metric to measure the difference between values and can be used to assess the accuracy of model predictions. The expression for RMSE is as follows:

$$\mathrm{RMSE} = \sqrt{\frac{\sum_{i=1}^{n}(y_i - \hat{y}_i)^2}{n}} \tag{12}$$

where n is the number of observations, y_i is the estimated value, and $\hat{y}_i$ is the actual value.

The calculations reveal that the RMSE for estimated displacement is 0.818 mm, and the RMSE for estimated velocity is 13.908 mm/s. The relative RMSE for estimated displacement is 7.91%, and the relative RMSE for estimated velocity is 21.41%.

3.3. Self-Sensing Combined with Kalman Filter Observer

Due to the high measurement accuracy of acceleration sensors, they can be used to measure acceleration signals at various positions in a vehicle. When placed on the vehicle body, they can also be used to evaluate ride comfort based on the data. The root mean square error (RMSE) of the velocity estimated through self-sensing is 13.908 mm/s, with a relative RMSE of 21.41%. A smaller relative RMSE indicates higher estimation accuracy. However, the velocity estimation accuracy is relatively low, which negatively impacts vibration reduction. Therefore, the Kalman filter is used to further improve velocity estimation accuracy. The self-sensing electromagnetic suspension combined with a Kalman filter observer is shown in Figure 10.

According to Newton's law of motion, the dynamic equation of a passive suspension can be expressed as follows:

$$\begin{cases} m_s\ddot{z}_s = -k_s(z_s - z_t) - c_s(\dot{z}_s - \dot{z}_t) \\ m_t\ddot{z}_t = -k_t(z_t - z_g) + k_s(z_s - z_t) + c_s(\dot{z}_s - \dot{z}_t) \end{cases} \tag{13}$$

In the equation, m_s is the vehicle body mass, m_t is the wheel mass, k_s is the spring stiffness coefficient, k_t is the equivalent stiffness coefficient of the tire, c_s is the system equivalent damping coefficient including the ball screw friction, z_s is the absolute displacement of the vehicle body, z_t is the absolute displacement of the wheel, and z_g is the road excitation.

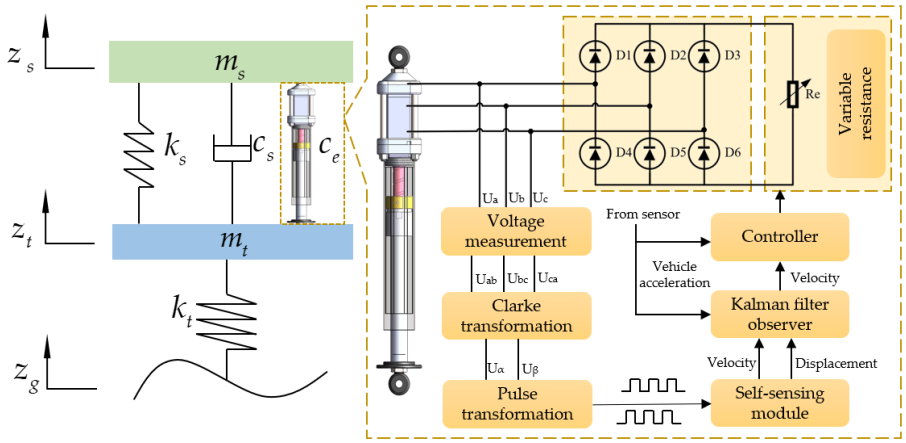

Figure 10. Self-sensing variable damping EMD suspension system.

The state vector and output vector of the system are $\boldsymbol{x} = \begin{bmatrix} z_s - z_t & z_t - z_g & \dot{z}_s & \dot{z}_t \end{bmatrix}^T$ and $\boldsymbol{y} = \begin{bmatrix} \ddot{z}_s & \dot{z}_s - \dot{z}_t & z_s - z_t \end{bmatrix}^T$, respectively.

Therefore, the state-space equation for the state-space variables can be written as in Equation (14):

$$\begin{cases} \dot{\boldsymbol{x}} = \boldsymbol{A}\boldsymbol{x} + \boldsymbol{B}\boldsymbol{u} + \boldsymbol{\Gamma}\boldsymbol{w} \\ \boldsymbol{y} = \boldsymbol{C}\boldsymbol{x} + \boldsymbol{D}\boldsymbol{u} + \boldsymbol{v} \end{cases} \tag{14}$$

In the equation,

$$\boldsymbol{A} = \begin{bmatrix} 0 & 0 & 1 & -1 \\ 0 & 0 & 0 & 1 \\ -\frac{k_s}{m_s} & 0 & -\frac{c_s}{m_s} & \frac{c_s}{m_s} \\ \frac{k_s}{m_t} & -\frac{k_s}{m_t} & \frac{c_s}{m_t} & -\frac{c_s}{m_t} \end{bmatrix}, \boldsymbol{B} = \begin{bmatrix} 0 \\ 0 \\ 0 \\ 0 \end{bmatrix}, \boldsymbol{\Gamma} = \begin{bmatrix} 0 \\ -1 \\ 0 \\ 0 \end{bmatrix}, \boldsymbol{C} = \begin{bmatrix} -\frac{k_s}{m_s} & 0 & -\frac{c_s}{m_s} & \frac{c_s}{m_s} \\ 0 & 0 & 1 & -1 \\ 1 & 0 & 0 & 0 \end{bmatrix},$$

$\boldsymbol{D} = \begin{bmatrix} 0 \\ 0 \\ 0 \end{bmatrix}$, u is the input variable, and w and v represent the assumed independent process Gaussian noise and observation Gaussian noise, respectively. $\boldsymbol{w} = \dot{z_g}$, z_g represents the rate of change of the road surface roughness velocity. $\boldsymbol{Q_k} = E(ww^T)$ and $\boldsymbol{R_k} = E(vv^T)$ are the corresponding process noise covariance and observation noise covariance, respectively.

The discrete expression required for computation based on the system's state-space equation is established as follows:

$$\begin{cases} \boldsymbol{x}_k = \boldsymbol{\Phi}\boldsymbol{x}_{k-1} + \boldsymbol{B'}\boldsymbol{u}_{k-1} + \boldsymbol{\Gamma'}\boldsymbol{w}_{k-1} \\ \boldsymbol{y}_k = \boldsymbol{H}\boldsymbol{x}_k + \boldsymbol{D'}\boldsymbol{u}_k + \boldsymbol{v}_k \end{cases} \tag{15}$$

where k represents the discrete time sampling instant.

Since the system is linear and the system noise follows a Gaussian distribution, the time update and measurement update equations of the Kalman filter algorithm can be easily derived [22].

Time Update ("Predict")

1. Project the state ahead:

$$\hat{\boldsymbol{x}}_{k+1}^{-} = \boldsymbol{\Phi}_k\hat{\boldsymbol{x}}_k + \boldsymbol{B'}\boldsymbol{u}_k \tag{16}$$

2. Project the error covariance ahead:

$$P_{k+1}^{-} = \Phi_k P_k \Phi_k^T + Q_k \tag{17}$$

Measurement Update ("Correct")

1. Compute the Kalman gain:

$$K_k = P_k^{-} H_k^T (H_k P_k^{-} P_k^T + R_k)^{-1} \tag{18}$$

2. Update estimate with measurement y_k:

$$\hat{x}_k = \hat{x}_k^{-} + K(y_k - H_k \hat{x}_k^{-}) \tag{19}$$

3. Update the error covariance:

$$P_k = (I - K_k H_k) P_k^{-} \tag{20}$$

As shown in Figure 10 the EMD is installed on the test bench to estimate the vehicle vibration state, verifying the filtering effect of the Kalman filter. As shown in Figure 11, the estimation performance of relative velocity under sinusoidal excitation is presented. Figure 11a shows the results under low-frequency sine excitation, while Figure 11b shows the results under high-frequency sine excitation. The SS-Estimate represents the performance of standalone self-sensing estimation, and the KFSS-Estimate represents the self-sensing estimation performance combined with a Kalman filter observer. As shown in Figure 12, under the condition of a Class C road at a speed of 40 km/h, the RMSE of relative velocity is 0.130 m/s for the SS-Estimate and 0.054 m/s for the KFSS-Estimate. Compared to standalone self-sensing, the self-sensing accuracy is improved by 58.46% when combined with the Kalman filter observer.

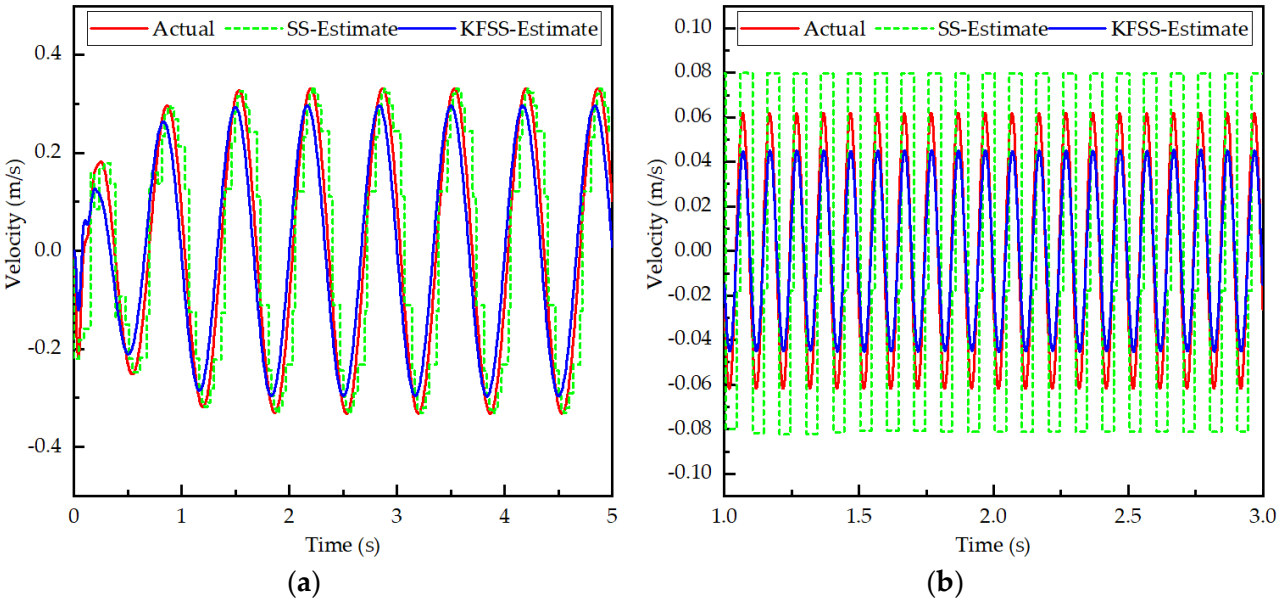

Figure 11. Comparison between estimated value and actual value under sine excitation: (**a**) 10 mm 1.5 Hz low-frequency sine; (**b**) 1 mm 10 Hz high-frequency sine.

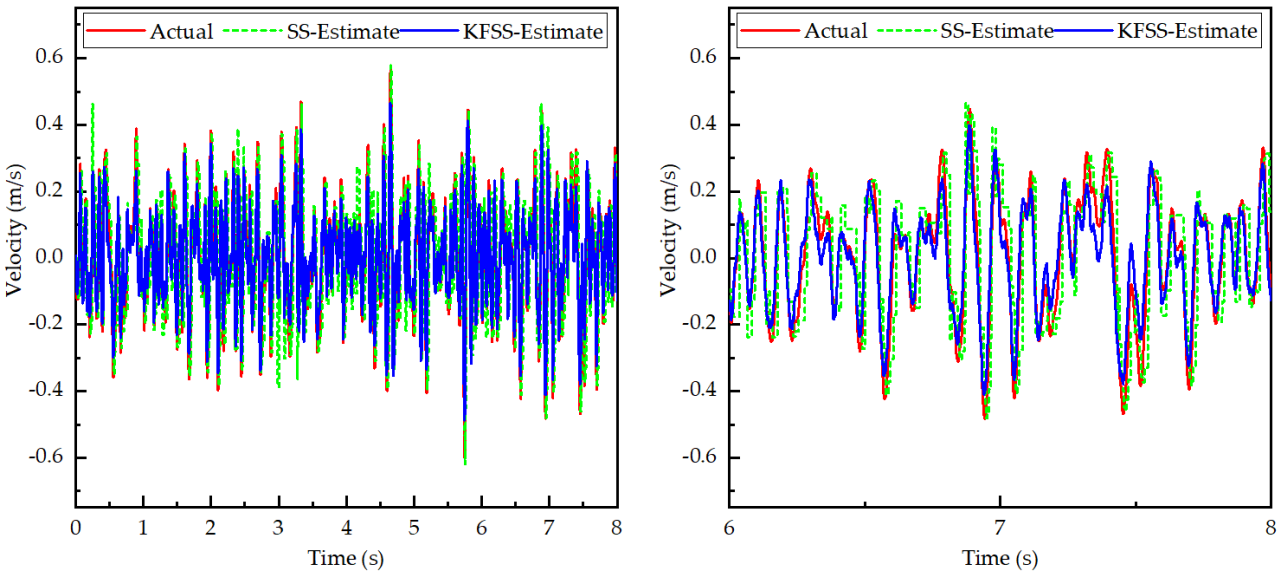

Figure 12. Comparison between estimated value and actual value.

4. Controller Design

The semi-active suspension is a complex nonlinear system with numerous influencing factors, making the control method one of the most important aspects. There are many types of semi-active control methods; commonly used ones include H∞ control [23], skyhook control [24], sliding mode control [25], and adaptive control [26]. In vehicle suspension system vibration control algorithms, the most straightforward and widely applied method is the skyhook control algorithm. Initially proposed by Karnopp in the United States, the skyhook control algorithm uses an imaginary damper connected to the skyhook to reduce vehicle body vibrations [27]. Similar to skyhook control, acceleration damping driven control (ADDC) assumes the presence of an ideal skyhook and uses an inertial container connected to the skyhook to suppress vehicle body vibrations, as shown in Figure 13a. This paper applies a variable resistance module to achieve variable damping in the semi-active suspension system, thereby providing the force required for ideal acceleration damping control. Figure 13b shows the one-quarter vehicle two-degree-of-freedom model of the electromagnetic suspension, where c_s represents the variable damping of the EMD. The values of these parameters in the EMS one-quarter vehicle model are listed in Table 1.

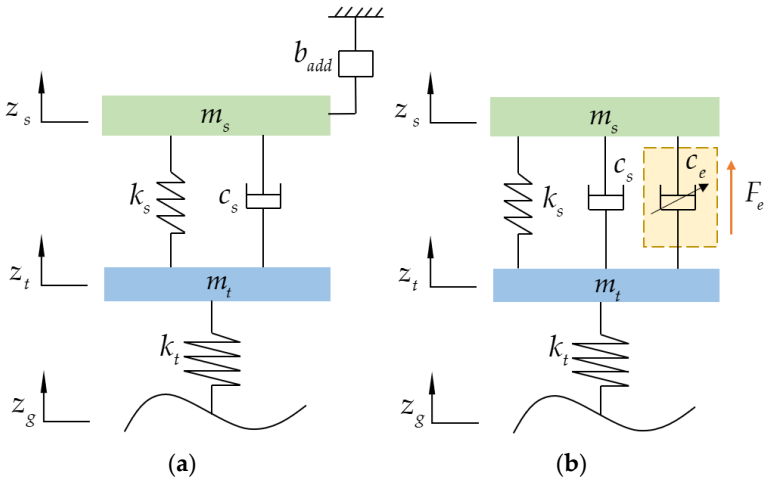

Figure 13. One-quarter vehicle 2-degree-of-freedom suspension system model: (**a**) ideal acceleration damping suspension; (**b**) EMS.

Table 1. Parameters of the quarter vehicle model with EMS.

Parameter	Symbol	Value
Vehicle mass	m_s	255 kg
Wheel mass	m_t	35 kg
Spring stiffness	k_s	21,000 N/m
Tire stiffness	k_t	200,000 N/m
Equivalent damping	c_s	1500 N·s/m
Ideal inertia	b_{add}	250 kg

According to Figure 13a, the differential equation for the suspension system is established as follows:

$$\begin{cases} m_s\ddot{z}_s = -k_s(z_s - z_t) - c_s(\dot{z}_s - \dot{z}_t) - b_{add}\ddot{z}_s \\ m_t\ddot{z}_t = -k_t(z_t - z_g) + k_s(z_s - z_t) + c_s(\dot{z}_s - \dot{z}_t) \end{cases} \tag{21}$$

The ideal inertial container connects the vehicle body to an imaginary skyhook rigidly. However, in practice, such a stationary skyhook cannot be provided. To address this, the ideal inertial container must be installed within the suspension system; for active control, the ideal input can be directly provided to the system by the actuator, $F_a = b_{add}\ddot{z}_s$. In the semi-active system studied here, the input force to the system is provided by the EMD, which achieves acceleration damping control through the adjustable damping of the electromagnetic suspension. According to Figure 13b, the differential equation for the EMS model can be written as follows:

$$\begin{cases} m_s\ddot{z}_s = -k_s(z_s - z_t) - c_s(\dot{z}_s - \dot{z}_t) + F_e \\ m_t\ddot{z}_t = -k_t(z_t - z_g) + k_s(z_s - z_t) + c_s(\dot{z}_s - \dot{z}_t) - F_e \end{cases} \tag{22}$$

As a semi-active actuator, the electromagnetic force provided by the EMD is essentially a damping force, in which direction can only be opposite to the relative motion, that is, $F_e = -c_e(\dot{z}_s - \dot{z}_t)$, where c_e represents the variable damping. After obtaining the ideal control force, which varies with the system's motion through control algorithms and system states, the electromagnetic force of the system is equated to the ideal control force. According to Equation (4), the following can be obtained:

$$F_a = -\frac{r_g^2 k_i^2}{r_i + R_e}(\dot{z}_s - \dot{z}_t) \tag{23}$$

Thus, the ideal variable damping resistance is given by

$$R_e = -\frac{r_g^2 k_i^2}{F_a}(\dot{z}_s - \dot{z}_t) - r_i \tag{24}$$

After obtaining the ideal resistance according to Equation (24), the closest one is extracted from among the 2^6 resistance levels of the system circuit structure. The controller adjusts the MOSFET switches to set the total external resistance to the indexed level, ensuring that the actual equivalent electromagnetic damping force produced by the EMD is as close as possible to the ideal force. This process is carried out at every moment in the system, allowing the EMD to provide an equivalent damping force that varies with the system's state during vibration. The basis for providing the damping force is to minimize the difference between the actual equivalent damping force and the desired ideal force, thus making the vibration situation as close as possible to the ideal case and achieving the vibration reduction goal.

The logic of the semi-active control strategy is shown in Figure 14.

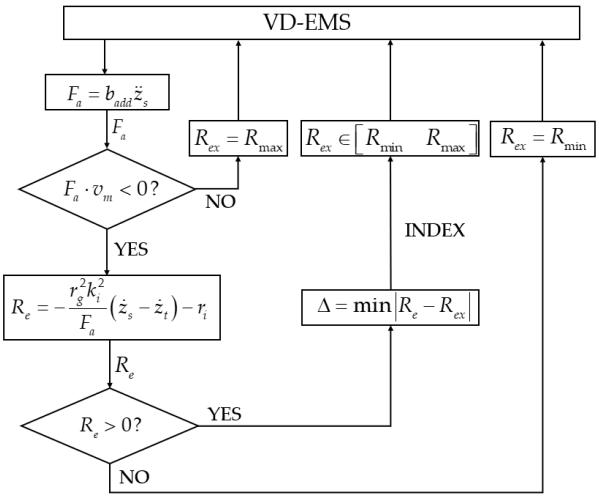

Figure 14. The control logic of the VD-EMS.

The ideal force F_a required for the system is calculated using the control algorithm. Since the actual equivalent damping force can only be in the opposite direction to the relative velocity, two cases can be considered:

1. When the ideal force is in the opposite direction to the relative velocity, the actual equivalent damping force will be in the same direction as the ideal force. In this case, by selecting the appropriate external resistance, the actual equivalent damping force can be set as close as possible to the ideal force, thereby ensuring that the system's vibration follows the pattern set by the control algorithm. It is important to note that due to the discrete nature of the external resistance used, the actual control resistance cannot be exactly equal to the ideal resistance. Therefore, the actual equivalent damping force cannot perfectly match the ideal force, but the difference can be minimized to make the vibration response as close as possible to the ideal case.
2. When the ideal force is in the same direction as the relative velocity, the actual equivalent damping force will necessarily be in the opposite direction to the ideal force. In this situation, the control will cause the vibration to worsen. At this point, the maximum resistance should be selected for the external resistor to minimize the actual equivalent damping force and ensure that the difference between the actual equivalent damping force and the ideal force is minimized, thereby reducing the degree of vibration deterioration. For the designed variable resistance module, using the maximum resistance ensures that the system's equivalent damping coefficient reaches a sufficiently low level, making the equivalent damping force close to 0; the degree of vibration deterioration can be almost ignored.

For the first case, after determining the required ideal resistance R_e, the closest external resistance combination R_{ex} is selected by indexing all resistance combinations in the external variable resistance module. For the second case, the maximum resistance $R_{\max}$ in the variable resistance module is used directly. By implementing these strategies, the control program and self-sensing estimation information can be utilized in real time to control the required resistance for the system. This allows for selecting the appropriate resistance level to adjust the EMD damping, thereby generating the equivalent electromagnetic damping force F_e, which is then input into the system to achieve semi-active vibration control.

5. Performance Evaluation Test

Applying self-sensing technology to semi-active control in electromagnetic suspension, the damping effect of the EMS is verified through experiments and evaluated by the vehicle's vertical acceleration value. In the experiment, the vibration-damping effects are tested by using the self-sensing estimated values as the observation values of ADDC and by using the sensor's measured values as the observation values of ADDC, respectively.

5.1. Introduction of the Test System

The EMS test system based on the one-quarter vehicle testing platform is illustrated in Figure 15. In the test system, the bottom is equipped with a retractable electric cylinder that provides excitation to simulate different driving conditions. The tire stiffness is equivalent to two high-stiffness springs, and above the tire springs is the wheel mass. The EMS springs are mounted on linear guide rails on both sides, with the vehicle body mass located above the suspension springs. An acceleration sensor and a displacement sensor are installed on the vehicle body to measure the body acceleration, suspension displacement, and suspension velocity. The upper and lower ends of the EMD are fixed to the test platform through specialized clamps. When the electric cylinder at the bottom generates excitation, it drives the vehicle body to move up and down, and the ball screw in the EMD converts the linear vertical motion into the rotational motion of the motor. Signal acquisition is performed using an NI cRIO, and a variable resistance module is connected to the circuit to achieve variable damping functionality.

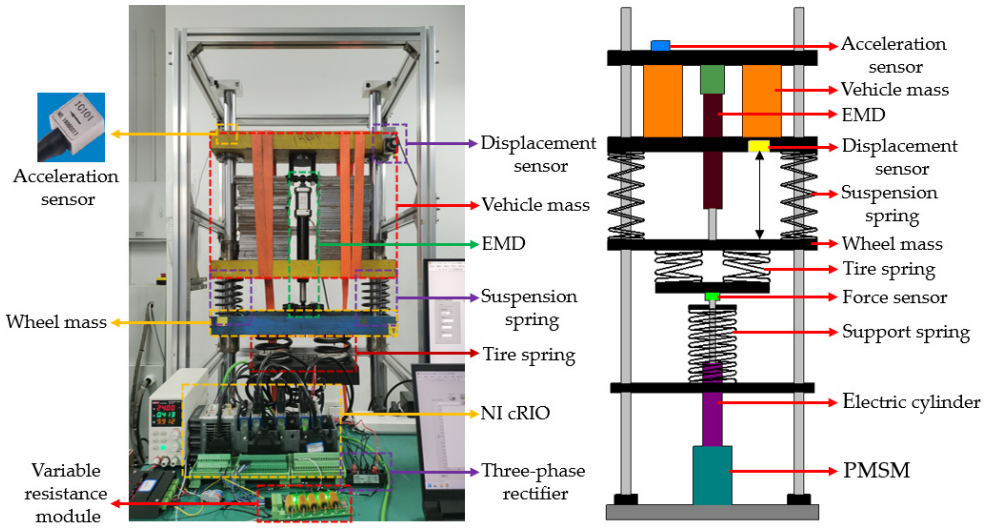

Figure 15. EMS test system.

5.2. Performance Evaluation Under Sine Excitation

A sinusoidal excitation is used as an ideal road input excitation. To facilitate a comparison between passive suspension and semi-active EMS, the sinusoidal excitation is applied to the wheel. In practical driving conditions, vehicles are predominantly subjected to low-frequency vibrations. The vehicle's natural frequency can be calculated using Equation (25).

$$f_0 = \frac{1}{2\pi}\sqrt{\frac{k_s}{m_s}} \tag{25}$$

Based on the values of the relevant parameters in Table 1, the vehicle's natural frequency can be determined, f_0 = 1.48 Hz, given a sinusoidal excitation, $x = 0.01\sin(3\pi t)$. Figure 16 shows the estimation performance of relative velocity under semi-active control conditions. As shown in Figure 17, under sinusoidal excitation, the EMD suspension can generate damping forces to reduce vehicle body vibrations. Comparing the vehicle's vertical acceleration in Figure 18, it can be seen that both the sensor measurement-controlled (referred to as ADDC) semi-active suspension and the self-sensing estimation-controlled (referred to as SS_ADDC) semi-active suspension reduce the vehicle's vertical acceleration. Calculations show that the root mean square (RMS) value of the vehicle vertical acceleration for the ADDC suspension is reduced by approximately 40.92%, while for the SS_ADDC suspension, it is reduced by about 43.31%. Similarly, comparing the suspension travel in Figure 19, both methods reduce the suspension travel, and the results are similar, with the peak suspension travel reduced by approximately 65%.

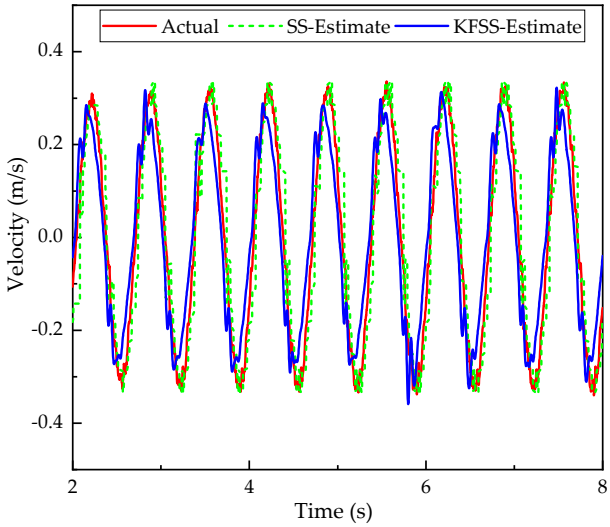

Figure 16. Comparison between estimated value and actual value under sine excitation.

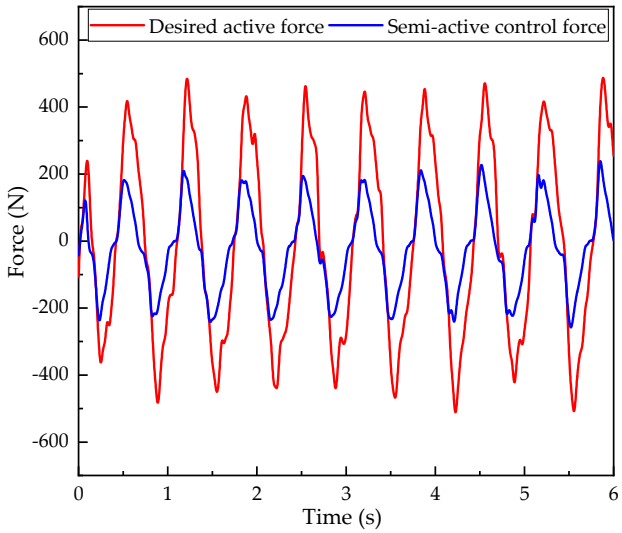

Figure 17. Force track performance under sine excitation.

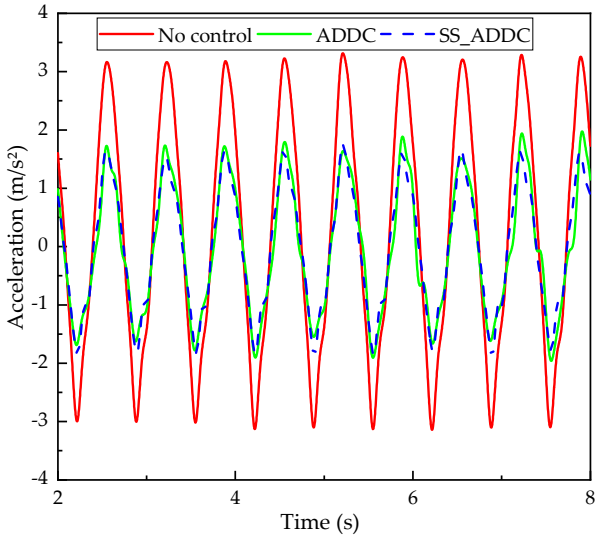

Figure 18. Vehicle vertical acceleration under sine excitation.

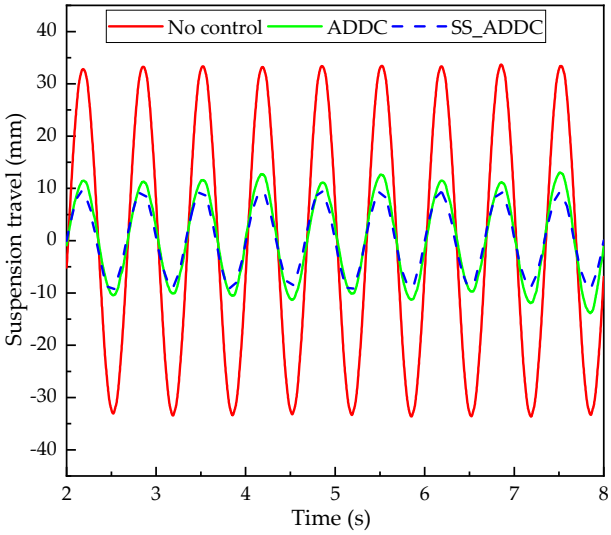

Figure 19. Suspension travel under sine excitation.

5.3. Performance Evaluation Under Random Road Excitation

To comprehensively evaluate the performance of the EMS system, random road excitation tests were conducted. The random road excitation was generated based on filtered white noise and a quarter-vehicle model. We compared the vehicle body vertical acceleration and suspension travel under the 40 km/h vehicle speed condition on a Class C road surface for different suspensions. Figure 20 shows the estimation performance of relative velocity under semi-active control conditions. As shown in Figure 21, under random road excitation, the EMD suspension can generate damping forces to reduce vehicle body vibrations. As shown in Figure 22, both the ADDC suspension and the SS_ADDC suspension effectively reduce the vehicle vertical acceleration, enhancing ride comfort. From the suspension travel comparison curve in Figure 23, it can be seen that the suspension travel of the ADDC suspension and SS_ADDC suspension is not significantly different from that of the passive suspension.

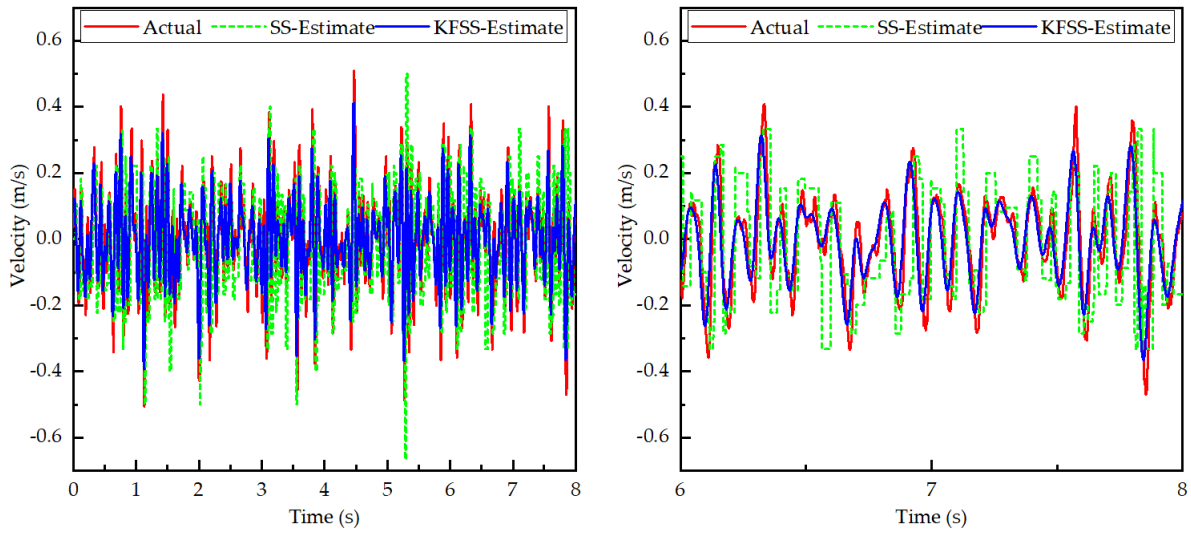

Figure 20. Comparison between estimated value and actual value under random road excitation.

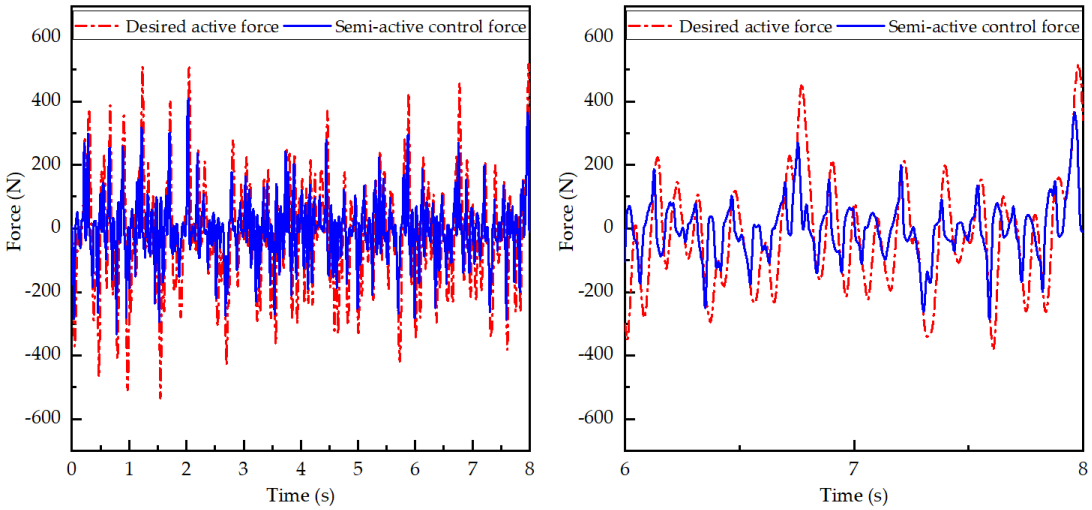

Figure 21. Force track performance under random road excitation.

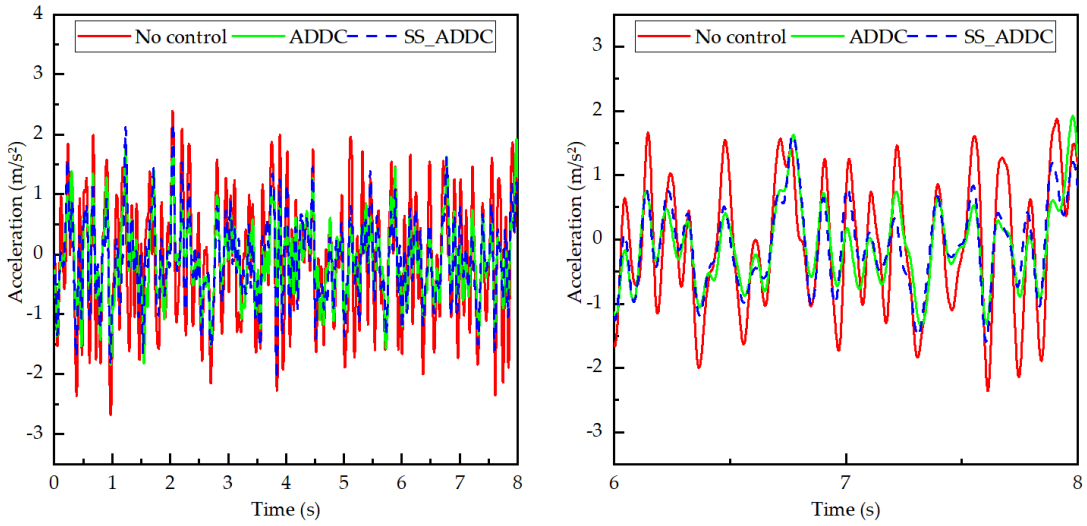

Figure 22. Vehicle vertical acceleration under random road excitation.

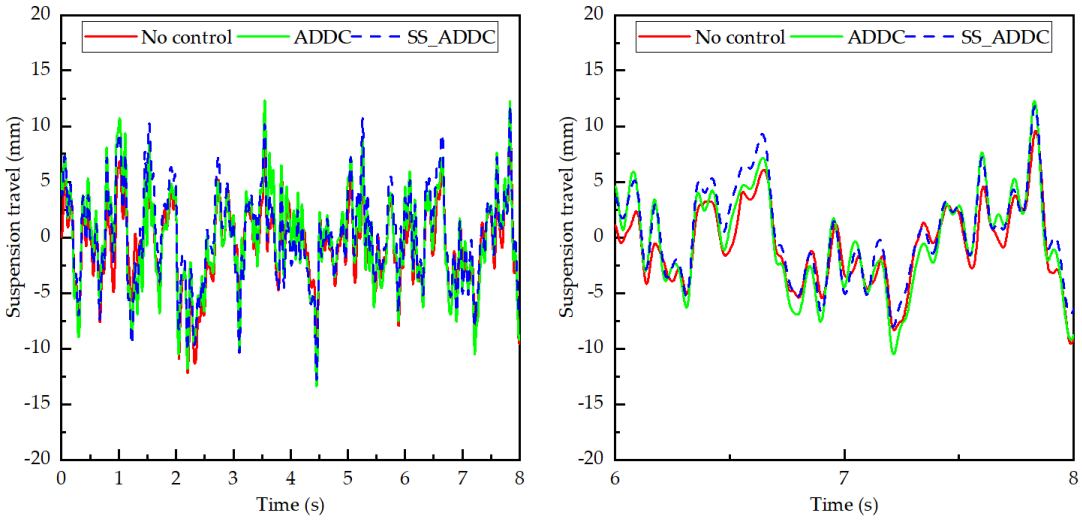

Figure 23. Suspension travel under random road excitation.

We quantified the percentage improvement in vibration performance of the EMS. According to the ISO 2631-1 standard [28], ride comfort is evaluated using the root mean square (RMS) of the vehicle body vertical acceleration, the frequency-weighted root mean square (FW-RMS), and the vibration dose value (VDV) to the fourth power. In Figure 24, the RMS, FWRMS, and VDV of each vehicle's vertical acceleration are displayed. Compared with the passive suspension, the RMS, FW-RMS, and VDV of the vertical acceleration of the ADDC suspension have reductions of 31.16%, 28.75%, and 26.88%. Compared with the passive suspension, due to the presence of errors in self-sensing, the performance indicators of the SS_ADDC suspension have reductions by 28.92%, 28.01%, and 28.18%, respectively.

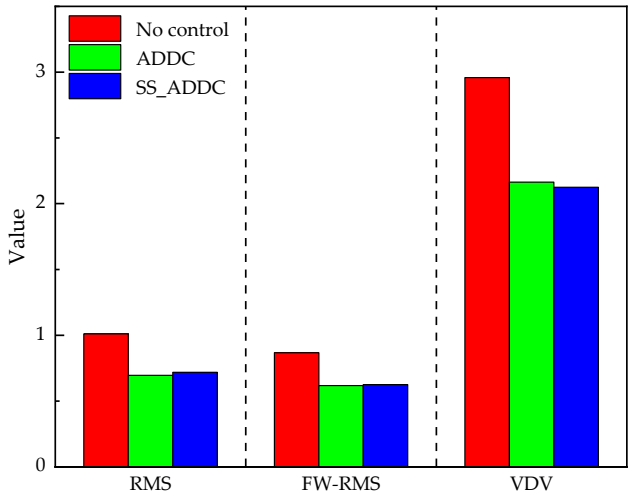

Figure 24. Evaluation parameters of vehicle vertical acceleration.

The above experimental results indicate that, compared to passive suspension, EMS can effectively reduce vibrations caused by road impacts, thus improving the vehicle's ride comfort to a certain extent. This also indicates that applying the self-sensing technology combined with the Kalman filter observer to the electromagnetic suspension for vibration control is feasible, and the control effect is comparable to that of the ADDC control.

6. Conclusions

This paper introduces a method for achieving semi-active control of the VD-EMS system using self-sensing technology, which reduces the need for external sensors. The accuracy of the self-sensing method and the effectiveness of the semi-active control in vibration reduction were validated through simulations and experiments. The main research results can be concluded as follows:

1. The variable-damping electromagnetic suspension system was designed, and the corresponding mathematical and physical models were established. The mechanism for achieving variable damping by altering the external circuit resistance was analyzed. This laid the foundation for the application of self-sensing technology in EMS.
2. We combined the Kalman filter observer with self-sensing technology to estimate the velocity and displacement of the electromagnetic suspension, and the accuracy of the estimation results was verified through experiments.
3. Parameters estimated through self-sensing were applied to the ADDC, to validate the effectiveness of an EMS in vibration. Applying self-sensing technology to vibration control in EMS is a feasible method.

This paper applies self-sensing technology to the semi-active control of EMS, thereby reducing the number of sensors, simplifying system complexity, and lowering the cost of the suspension system. Currently, self-sensing technology still has some errors, leading to fluctuations in the vibration reduction effect. Future research will focus on addressing the errors present in self-sensing technology and applying this method to the full vehicle

suspension system. More advanced controllers will be utilized to enhance the performance of the EMS system.

Author Contributions: Conceptualization, C.F., D.N. and J.Y.; methodology, P.L. and A.Q.; validation, C.F. and P.L.; writing—original draft preparation, C.F.; writing—review and editing, P.L. and D.N.; supervision, D.N.; experiments, C.F. and P.L. All authors have read and agreed to the published version of the manuscript.

Funding: This research was funded by the China Postdoctoral Science Foundation (Grant No. 2023M733339), the Nature Science Foundation of Shandong Project (Grant No. ZR2023QE113) and Taishan Scholars Program of Shandong Province (Grant No. tsqn202211062).

Data Availability Statement: No data need to be reported.

Conflicts of Interest: The authors declare no conflicts of interest.

References

1. Masa'id, A.; Lenggana, B.W.; Ubaidillah, U.; Susilo, D.D.; Choi, S.-B. A Review on Vibration Control Strategies Using Magnetorheological Materials Actuators: Application Perspective. *Actuators* **2023**, *12*, 113. [CrossRef]
2. Floreán-Aquino, K.H.; Arias-Montiel, M.; Linares-Flores, J.; Mendoza-Larios, J.G.; Cabrera-Amado, Á. Modern Semi-Active Control Schemes for a Suspension with MR Actuator for Vibration Attenuation. *Actuators* **2021**, *10*, 22. [CrossRef]
3. Roshan, Y.M.; Maravandi, A.; Moallem, M. Power Electronics Control of an Energy Regenerative Mechatronic Damper. *IEEE Trans. Ind. Electron.* **2015**, *62*, 3052–3060. [CrossRef]
4. Zhang, Z.; Qin, A.; Zhang, J.; Zhang, B.; Fan, Q.; Zhang, N. Fuzzy sampled-data H∞ sliding-mode control for active hysteretic suspension of commercial vehicles with unknown actuator-disturbance. *Control Eng. Pract.* **2021**, *117*, 104940–104953. [CrossRef]
5. Mai, V.N.; Yoon, D.-S.; Choi, S.-B.; Kim, G.-W. Explicit model predictive control of semi-active suspension systems with magnetorheological dampers subject to input constraints. *J. Intell. Mater. Syst. Struct.* **2020**, *31*, 1157–1170. [CrossRef]
6. Liu, P.; Xia, X.; Zhang, N.; Ning, D.; Zheng, M. Torque response characteristics of a controllable electromagnetic damper for seat suspension vibration control. *Mech. Syst. Signal Process.* **2019**, *133*, 106238–106254. [CrossRef]
7. Zare, K.; Mardani, M.M.; Vafamand, N.; Khooban, M.H.; Sadr, S.S.; Dragičević, T. Fuzzy-logic-based adaptive proportional-integral sliding mode control for active suspension vehicle systems: Kalman filtering approach. *Inf. Technol. Control* **2019**, *48*, 648–659. [CrossRef]
8. Zhang, J.; Ding, F.; Zhang, N.; Chen, S.; Zhang, B. A New SSUKF Observer for Sliding Mode Force Tracking H∞ Control of Electrohydraulic Active Suspension. *Asian J. Control* **2020**, *22*, 761–778. [CrossRef]
9. Ren, H.; Chen, S.; Zhao, Y.; Liu, G.; Yang, L. State observer-based sliding mode control for semi-active hydro-pneumatic suspension. *Veh. Syst. Dyn.* **2016**, *54*, 168–190. [CrossRef]
10. Pan, H.; Sun, W.; Gao, H.; Hayat, T.; Alsaadi, F. Nonlinear tracking control based on extended state observer for vehicle active suspensions with performance constraints. *Mechatronics* **2015**, *30*, 363–370. [CrossRef]
11. Wang, H.; Kin Wong, P.; Zhao, J.; Yang, Z.-X.; Yang, Z.-X. Observer-based robust gain-scheduled control for semi-active air suspension systems subject to uncertainties and external disturbance. *Mech. Syst. Signal Process.* **2022**, *173*, 109045–109065. [CrossRef]
12. Zhang, B.; Liu, M.; Wang, K.; Tan, B.; Deng, Y.; Qin, A.; Liu, J. Takagi–Sugeno Fuzzy Model-Based Control for Semi-Active Cab Suspension Equipped with an Electromagnetic Damper and an Air Spring. *Machines* **2023**, *11*, 226. [CrossRef]
13. Xia, X.; Zheng, M.; Liu, P.; Zhang, N.; Ning, D.; Du, H. Friction observer-based hybrid controller for a seat suspension with semi-active electromagnetic damper. *Mechatronics* **2021**, *76*, 102568. [CrossRef]
14. Shi, Q.; Zhang, H. An Improved Control-Oriented Tire Model and Its Applications on Intelligent Vehicles. *IEEE Trans. Intell. Veh.* **2024**, *9*, 1501–1511. [CrossRef]
15. Qin, A.; Zhang, B.; Ning, D.; Tan, B.; Du, H. A self-sensing approach for estimating suspension displacement and velocity in semi-active electromagnetic dampers. *Mech. Syst. Signal Process.* **2024**, *208*, 111049. [CrossRef]
16. Verma, M.; Lafarga, V.; Collette, C. Perfect collocation using self-sensing electromagnetic actuator: Application to vibration control of flexible structures. *Sens. Actuators A Phys.* **2020**, *313*, 112210. [CrossRef]
17. Yao, Y.; Li, Y.; Yin, Q. A novel method based on self-sensing motor drive system for misalignment detection. *Mech. Syst. Signal Process.* **2019**, *116*, 217–229. [CrossRef]
18. Hu, G.; Ru, Y.; Li, W. Design and development of a novel displacement differential self-induced magnetorheological damper. *J. Intell. Mater. Syst. Struct.* **2014**, *26*, 527–540. [CrossRef]
19. Deng, H.; Gao, Y.; Hu, R.; Zhao, S.; Han, G.; Lian, X.; Ma, M.; Zhong, X. Self-sensing automotive magnetorheological dampers for low frequency vibration. *Smart Mater. Struct.* **2021**, *30*, 115015. [CrossRef]
20. Zhang, Z.; Zhang, X.; Chen, W.; Rasim, Y.; Salman, W.; Pan, H.; Yuan, Y.; Wang, C. A high-efficiency energy regenerative shock absorber using supercapacitors for renewable energy applications in range extended electric vehicle. *Appl. Energy* **2016**, *178*, 177–188. [CrossRef]

21. Maciejewski, I.; Zlobinski, M.; Krzyzynski, T.; Glowinski, S. Vibration control of an active horizontal seat suspension with a permanent magnet synchronous motor. *J. Sound Vib.* **2020**, *488*, 115655–115671. [CrossRef]
22. Khodarahmi, M.; Maihami, V. A review on Kalman filter models. *Arch. Comput. Methods Eng.* **2023**, *30*, 727–747. [CrossRef]
23. Ning, D.; Du, H.; Sun, S.; Li, W.; Li, W. An Energy Saving Variable Damping Seat Suspension System With Regeneration Capability. *IEEE Trans. Ind. Electron.* **2018**, *65*, 8080–8091. [CrossRef]
24. Liu, C.; Chen, L.; Yang, X.; Zhang, X.; Yang, Y. General Theory of Skyhook Control and its Application to Semi-Active Suspension Control Strategy Design. *IEEE Access* **2019**, *7*, 101552–101560. [CrossRef]
25. Chen, B.-C.; Shiu, Y.-H.; Hsieh, F.-C. Sliding-mode control for semi-active suspension with actuator dynamics. *Veh. Syst. Dyn.* **2011**, *49*, 277–290. [CrossRef]
26. Ding, Z.; Zhao, F.; Qin, Y.; Tan, C. Adaptive neural network control for semi-active vehicle suspensions. *J. Vibroeng.* **2017**, *19*, 2654–2669. [CrossRef]
27. Williams, D.E. Active suspension: Future lessons from the past. *SAE Int. J. Veh. Dyn. Stab. NVH* **2018**, *2*, 147–165. [CrossRef]
28. ISO. *Mechanical Vibration and Shock-Evaluation of Human Exposure to Whole-Body Vibration—Part 1: General Requirements*; ISO: Geneva, Switzerland, 2010.

Disclaimer/Publisher's Note: The statements, opinions and data contained in all publications are solely those of the individual author(s) and contributor(s) and not of MDPI and/or the editor(s). MDPI and/or the editor(s) disclaim responsibility for any injury to people or property resulting from any ideas, methods, instructions or products referred to in the content.